GEOPHYSICAL RESEARCH LETTERS, VOL. 27, NO. 18, PAGES 2945-2948, SEPTEMBER 15, 2000

Climatology and Seasonal Variability of Ocean Fronts in the East China, Yellow and Bohai Seas From Satellite SST Data

Ryan Hickox, Igor Belkin, Peter Cornillon, and Zhengqiang Shan

Graduate School of Oceanography, University of Rhode Island, Narragansett, Rhode Island

Abstract. Front detection and declouding algorithms developed at the URI have been applied to the 12-year (1985-1996) Pathfinder SST data set to produce the first comprehensive, objectively derived, year-round climatology of ocean thermal fronts in the eastern China Seas, from 24°N to 41°N. Ten fronts have been distinguished, namely Kuroshio, Zhejiang-Fujian, Jiangsu, Shandong Peninsula, Bohai Sea, Seohan Bay, Kyunggi Bay, Western and Eastern Chejudo (South Korean Coastal Front), and Yangtze Bank Ring Front. The fronts are seasonally persistent: they emerge and disappear in the same seasons of different years. The frontal pattern remains fairly stable from one year to another, whereas individual fronts display different modes of seasonal variability.

Introduction

The eastern China Seas lie between China, Korea and Japan, from 24°N to 41°N (Figure 1). Three marginal seas are distinguished here (from south to north): the East China Sea, Yellow Sea, and Bohai Sea. These seas (ECYB Seas hereafter) are closely related and share features of the monsoon-dominated climate, circulation, and water mass formation [*Su*, 1998].

The sea surface temperature (SST) fronts in the ECYB Seas have been studied from remotely-sensed data since the 1970s. Huh [*Huh*, 1976, 1982] used satellite data to describe coastal fronts off Korea. Zheng [*Zheng*, 1981] and Zheng and Klemas [*Zheng and Klemas*, 1982] attempted the first comprehensive studies of the ECYB Seas fronts, based on wintertime SST data. He et al.[*He et al.*, 1995] have identified major fronts in the ECYB Seas from the SST imagery for 1984-1989. Ning et al.[*Ning et al.*, 1998] used the SST data from 1981-1986 to distinguish thermal fronts and correlate them with color scanner data.

This study adds to the literature in several ways. First, the data are used to distinguish ten frontal regions, based on the location of the fronts and on their temporal evolution. Second, the probability of frontal occurence is estimated at each location. Third, the seasonal variability of the probability density field is analyzed.

Paper number 1999GL011223.
0094-8276/00/1999GL011223$05.00

Developing Frontal Probability Distributions

The fronts used for this study were derived from the NOAA/NASA Pathfinder SST "all-pix" (i.e., no cloud mask) fields [*Vazquez et al.*, 1998] for the period 1985-1996. These fields were obtained from the AVHRR Global Area Coverage data stream (9.28 km fields per day) and are available from the Jet Propulsion Laboratory (JPL).

Prior to applying the edge detection algorithm to the Pathfinder SST fields, it was necessary to flag cloud contaminated pixels to avoid the detection of false fronts at the edge of cloud covered regions. The cloud-detection algorithm developed by Cayula and Cornillon [*Cayula and Cornillon*, 1996] was used for this step rather than acquiring the cloud masked images from JPL because the Pathfinder cloud masking algorithm is based on the homogeneity of the SST field hence tends to flag pixels in the vicinity of strong fronts as cloud contaminated. The Cayula and Cornillon algorithm has been designed to work with the front detection algorithm, hence to minimize this problem.

SST fronts were obtained from the cloud masked SST fields with the multi-image edge detection algorithm developed by Cayula and Cornillon [*Cayula and Cornillon*, 1995]. This algorithm is histogram based as opposed to gradient based which is significant for the detection of weak (small SST step over a short distance) fronts. For strong fronts the error rates, both for false detections and for missed fronts, are similar for histogram and gradient based algorithms [*Ullman and Cornillon*, 1999]. For weak fronts however, setting the gradient threshold so that the error rate for missed fronts is the same for both algorithm types, results in a significantly higher rate of false front detection for gradient algorithms. Conversely, setting the gradient threshold so that the error rate for false detections is the same for both algorithm types results in a significantly higher rate of missed fronts with gradient algorithms.

The cloud masking and front detection algorithms were applied to each of the 8364 SST images in the 12 year sequence. Because cloud cover results in irregular coverage of the study region from one image to the next, interpretation of the frontal distribution for individual images is difficult. The frontal data were therefore aggregated over periods for which the statistical distribution of fronts was stable. For this study, intervals used were climatological months (12 Januaries taken together, 12 Februaries taken together,.), climatological seasons (e.g., the spring climatology is obtained from all Aprils, Mays and Junes taken together), and the entire 12 year period. For each of these intervals, images of the probability that a pixel was a frontal pixel were derived from the data by dividing the number of times the

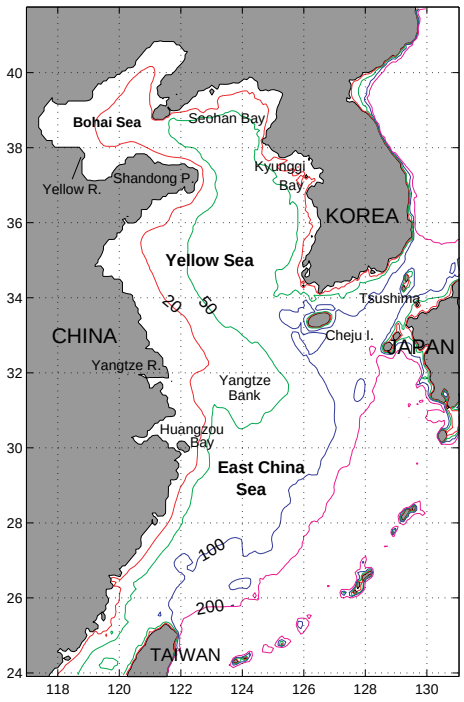

Figure 1. Study area.

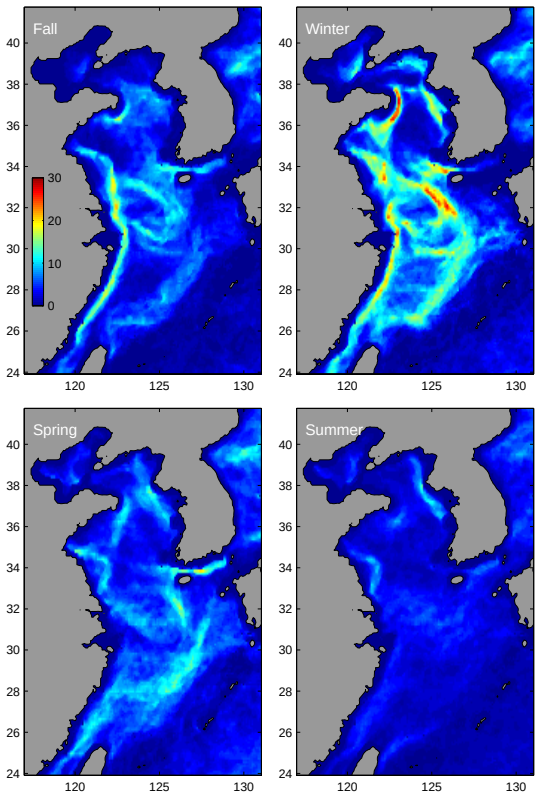

Figure 3. Seasonal frontal probability maps for 1985-1996.

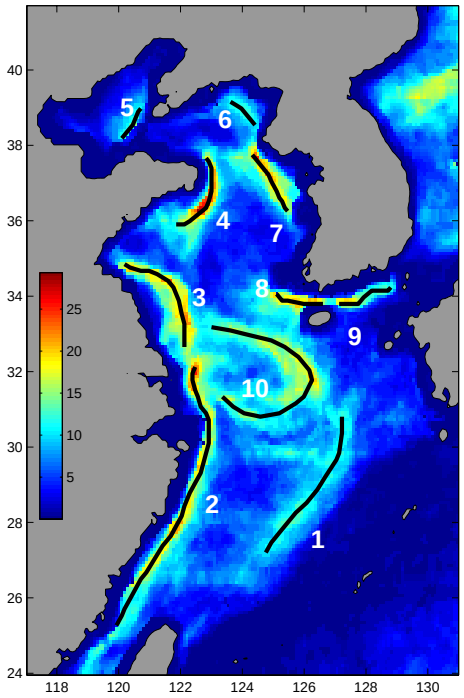

Figure 2. Long-term annual composite frontal probability map for the 1985-1996 period. For each pixel, shown is the percentage of the total time that the given pixel contained a front. The rainbow insert is the percentage scale. Solid black lines mark maximum probability ridges that correspond to most probable locations of fronts. Numbers are: 1, Kuroshio Front; 2, Zhejiang-Fujian Front; 3, Jiangsu Front; 4, Shandong Peninsula Front; 5, Bohai Sea Front; 6, Seohan Bay Front; 7, Kyunggi Bay Front; 8, Western Chejudo Front; 9, Eastern Chejudo Front; 10, Yangtze Bank Ring Front.

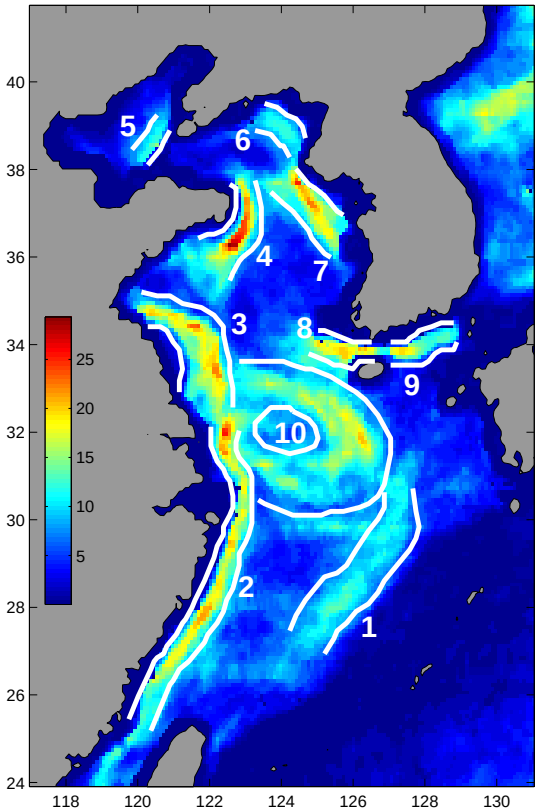

Figure 4. Frontal boundaries used to determine cross-frontal SST ranges.

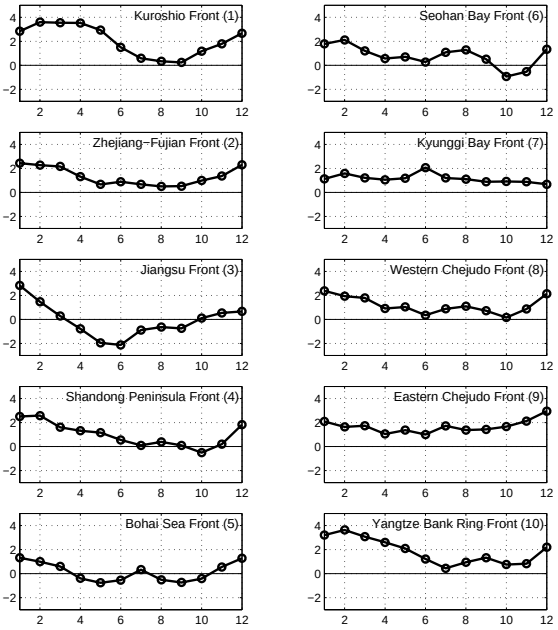

Figure 5. Seasonal variability of cross-frontal SST differences $DT = T_{offshore} - T_{onshore}$.

pixel was a frontal pixel for the interval of interest by the number of times the pixel was clear for the same interval.

Ten fronts are evident in the 12-year probability image of the region (Figure 2), namely: 1, Kuroshio Front; 2, Zhejiang-Fujian Front; 3, Jiangsu Front; 4, Shandong Peninsula Front; 5, Bohai Sea Front; 6, Seohan Bay Front; 7, Kyunggi Bay Front; 8, Western Chejudo Front; 9, Eastern Chejudo Front; and 10, Yangtze Bank Ring Front, where the numbers preceding the front's name correspond to the numbers in Figure 2.

Seasonal Variability of the Frontal Pattern

The frontal pattern of the ECYB Seas is strongly seasonal. Most fronts emerge in fall and winter, fade in spring and almost disappear in summer (Figure 3). Monthly frontal probability maps [*Belkin et al.*, 1999] reveal the entire frontal pattern of the ECYB Seas to be best seen from November through April. In late spring and in summer, seasonal surface warming smoothes the SST field; only the Jiangsu, Seohan Bay and Kyunggi Bay fronts are clearly visible in late summer. In fall, the Kuroshio Front is distinct again. The Zhejiang-Fujian Front appears and connects to the Jiangsu Front to form the continuous China Coastal Front from the Taiwan Strait north to 35°N. The Shandong Peninsula Front forms and extends around the Peninsula. A remarkable oval-shaped ("ring") front develops around the Yangtze Bank. The Eastern Chejudo Front emerges, followed by the Western Chejudo Front. The winter pattern is similar to late fall except for the newly formed Bohai Sea, Seohan Bay, and Kyunggi Bay fronts. In spring, the Zhejiang-Fujian Front weakens, detaches from the Jiangsu Front and joins the Kuroshio Front NNE of Taiwan, while the Jiangsu Front merges with remnants of the Yangtze Bank Ring Front to form a horseshoe front across the entire basin. The Shandong Peninsula Front fades. The Seohan Bay Front is visible on and off. The Eastern Chejudo Front grows stronger, while the Western Chejudo Front weakens and disappears.

Seasonal Variability of Individual Fronts

To study seasonal variability of individual fronts, we have calculated SST ranges across each front as follows. First, the annual frontal probability composite map (Figure 2) was used to determine approximate boundaries of each frontal zone (Figure 4). Then, using the Pathfinder monthly SST climatology developed by Casey and Cornillon [*Casey and Cornillon*, 1999], the mean monthly SST along these boundaries were calculated. This gives long-term mean monthly SST estimates for the offshore ($T_{offshore}$) and onshore ($T_{onshore}$) sides of each front and for the cross-frontal SST differences $DT = T_{offshore} - T_{onshore}$ (Figure 5).

Figure 5 displays the cross-frontal SST steps (DT) as a function of climatological month for each of the 10 fronts. Most fronts have larger SST steps in winter, apparently because of the masking effect of the summertime warming. The Kuroshio Front displays a quasi-sinusoidal seasonal trend. Other fronts' trends are qualitatively different. Out of ten fronts identified, most (seven) fronts are coastal, namely the Zhejiang-Fujian, Jiangsu, Shandong Peninsula, Seohan Bay, Kyunggi Bay, Western Chejudo and Eastern Chejudo fronts. Some coastal fronts are colder on the onshore side and warmer on the offshore side, year-round. Other fronts' cross-frontal differences change sign as the season progresses, namely the Jiangsu, Shandong Peninsula, Bohai Sea and Seohan Bay fronts. The Shandong Peninsula, Seohan Bay, Western Chejudo and Yangtze Bank Ring fronts display very similar seasonal trends. It's noteworthy that these fronts follow the 50-m isobath. The newly identified Bohai Sea Front is best seen in winter when DT peaks at 1.3°C. Seasonal trends of the Korean coastal fronts (# 6 through 9) are qualitatively different. Some workers identify a single continuous front west of the Korean Peninsula [*Ning et al.*, 1998]. We differentiated, however, between the Seohan Bay and Kyunggi Bay fronts because we found their characteristics to be distinctly different. The fronts have non-overlapping SST ranges from January through May, the Kyunggi Bay Front being much warmer then the Seohan Bay Front. In addition, the seasonal trends of the cross-frontal SST steps differs (Figure 5), for these two fronts. We also found significant differences between the Western and Eastern Chejudo Fronts (Figure 5). The former becomes very weak in summer while the latter remains fairly strong year-round. The remarkable Yangtze Bank Ring Front was found to surround a cold region, with the cross-frontal step DT up to 4°C in winter (Figure 5).

Summary and Conclusions

This study has produced the first comprehensive, objectively derived, year-round climatology of ocean thermal fronts in the eastern China Seas. All the previously known fronts have been reliably identified. A newly found front in the Bohai Sea was described. The China Coastal Front consists of two fronts that merge and split as the season progresses. Off the Korean Peninsula, four fronts have been distinguished with qualitatively different seasonal characteristics. All of the observed fronts are seasonally persistent, and the frontal pattern remains fairly stable despite distinctly different seasonal variability of individual fronts.

Acknowledgments. The research was supported by the NASA Grant No. 535834. The work of R. Hickox at the Graduate School of Oceanography, URI, was part of the SURFO program, funded by the NSF. The image processing software was developed by R. Evans, O. Brown, J. Brown, and A. Li of the University of Miami.

References

Belkin, I. M., R. Hickox, P. Cornillon, and Z. Shan, Ocean fronts in the East China, Yellow, and Bohai Seas from satellite and in situ data, in preparation, 1999.

Casey, K. S., and P. Cornillon, A comparison of satellite and in situ based sea surface temperature climatologies, *J. Climate, 12*, 1848-1863, 1999.

Cayula, J.-F., and P. Cornillon, Multi-image edge detection of SST images, *J. Atmos. Oceanic. Technol., 12*, 821-829, 1995.

Cayula, J.-F., and P. Cornillon, Cloud detection from a sequence of SST images, *Remote Sens. Environ., 55*, 80-88, 1996.

He, M. X., G. Chen, and Y. Sugimori, Investigation of mesoscale fronts, eddies and upwelling in the China Seas with satellite data, *Global Atmosphere and Ocean System, 3*, 273-288, 1995.

Huh, O. K., Detection of oceanic thermal fronts off Korea with the defense meteorological satellite, *Remote Sensing of Environment, 5*, 191-213, 1976.

Huh, O. K., Satellite observations and the annual cycle of surface circulation in the Yellow Sea, East China Sea, and Korea Strait, *La Mer, 20*, 210-222, 1982.

Ning, X., Z. Liu, Y. Cai, M. Fang, F. Chai, Physicobiological oceanographic remote sensing of the East China Sea: Satellite and in situ observations, *J. Geophys. Res., 103*, 21623-21635, 1998.

Su, J., Circulation dynamics of the China Seas north of 18°N, in *The Global Coastal Ocean, Volume 11: Regional Studies and Syntheses,* edited by A.R. Robinson and K.H. Brink, pp. 483-505, John Wiley & Sons, New York etc., 1998.

Ullman, D.S., and P.C. Cornillon, Surface temperature fronts off the East Coast of North America from AVHRR imagery, *J. Geophys. Res., 104*, 23,459-23,478, 1999.

Vazquez, J., K. Perry, and K. Kilpatrick, NOAA/NASA AVHRR Oceans Pathfinder sea surface temperature data set user's reference manual, Version 4.0, *JPL Technical Report, D14070, http://podaac.jpl.nasa.gov/ pub/ sea_surface_temperature/ avhrr/ pathfinder/ doc/ usr_gde4_0.html,* 1998

Zheng, Q., The winter surface temperature pattern of the Huanghai Sea and the East China Sea derived from the GMS-1 and NOAA-5 satellite IR images, *Acta Oceanologica Sinica, 3*, 524-534, 1981.

Zheng, Q., and V. Klemas, Determination of winter temperature patterns, fronts, and surface currents in the Yellow Sea and East China Sea from satellite imagery, *Remote Sensing of Environment, 12*, 201-218, 1982.

R. Hickox and I. M. Belkin and P. C. Cornillon and Z. Shan, Graduate School of Oceanography, University of Rhode Island, 215 South Ferry Road, Narragansett, RI 02882. (e-mail: ibelkin@gso.uri.edu)

(Received November 1, 1999; accepted May 11, 2000)